The Kinetics of the Internal Nitriding of Fe-2 At. Pct Al Alloy

M.H. BIGLARI, C.M. BRAKMAN, E.J. MITTEMEIJER, and S. VAN DER ZWAAG

The kinetics of the precipitation of aluminum nitride on internal nitriding the Fe-2 at. pct Al alloy was investigated for cold-rolled and recrystallized specimens exhibiting "ideally weak" interaction behavior of the solutes Al and N. The kinetic analysis was performed using mass-increase data obtained for thin foils (thickness ≤ 0.1 mm) upon nitriding in a NH_3/H_2 gas mixture at temperatures in the range 803 to 853 K. Activation-energy analysis revealed that precipitation of AlN in the recrystallized specimens is associated with a Gibbs free energy barrier for the formation of a precipitate of critical size; the precipitation rate is controlled by both nucleation and growth. On the other hand, precipitation of AlN in the cold-rolled specimens occurs without a Gibbs free energy barrier for formation of a precipitate of critical size; the precipitation rate is controlled by growth with kinetics governed by volume diffusion of aluminum. Analysis of the total Gibbs free energy of formation of AlN in the α-Fe matrix showed that in the case of the recrystallized specimens, the formation of incoherent AlN precipitates with a hexagonal crystal structure is favored. In the case of the cold-rolled specimens, containing a high dislocation density, the formation of coherent AlN precipitates with cubic crystal structure is favored, at least in the beginning of precipitation.

I. INTRODUCTION

INTERNAL nitriding of ferritic steels is performed to enhance the fatigue resistance and also to improve the wear properties. The improvement of properties is due to the formation of a so-called diffusion zone[1] where the nitriding-induced strengthening is caused by the precipitation of very small particles of nitride(s) of the alloying element(s), like aluminum[2–5] and chromium.[6–12] Models allowing reliable quantitative predictions of the properties after nitriding do not exist at present. This is caused by a lack of knowledge on the (kinetics of the) microstructural changes evoked in the nitrided region. The present project aims at the development of such models for the case of aluminum as an alloying element in iron and steels. An Fe-2 at. pct Al alloy has been chosen as the model system. The microstructure after nitriding has been discussed in Reference 5. The present article deals in particular with the kinetics of the internal nitriding of Fe-2 at. pct Al specimens. The effects of two initially different specimen conditions have been studied: recrystallized and cold-rolled.

Thermogravimetric gaseous nitriding experiments of flat, thin specimens have been performed to extract kinetic parameters from mass-increase data obtained as a function of time and temperature. Each mass-increase data point represents the total momentary nitrogen uptake of the specimen or, in other words, the value of the nitrogen uptake averaged over all depths in the specimen. For straightforward interpretation of the thermobalance data, the local nitrogen uptakes should represent ideally weak interaction behavior of the solutes Al and N.[5] Ideally weak interaction behavior implies that during nitriding the nitrogen concentration is constant as a function of distance to the surface. This implies that (upon nitriding) nitrogen can reach the core of the specimen by diffusion before significant nitride precipitation occurs near the surface. Continued nitriding then corresponds with a gradual increase of the homogeneous nitrogen level of the specimen. This condition is realized here by application of sufficiently thin foils.

M.H. BIGLARI, Ph.D. Student, C.M. BRAKMAN, Senior Researcher, and E.J. MITTEMEIJER and S. VAN DER ZWAAG, Professors, are with the Laboratory of Materials Science, Delft University of Technology, Rotterdamseweg 137, 2628 AL, Delft, The Netherlands.

Manuscript submitted March 24, 1994.

II. EXPERIMENTAL

The Fe-Al alloy used was prepared by melting iron and aluminum powder under an H_2 flow in a sintered Al_2O_3 crucible. The composition of the Fe-Al alloys is given as follows: 2.05 at. pct Al, 4×10^{-4} at. pct N, 6×10^{-3} at. pct C, 6×10^{-3} at. pct O, balance Fe.

The Fe-Al bar was cold-rolled down to a final thickness of ≈ 0.15 mm, applying recrystallization treatments at 973 K in Ar after ≈ 65 pct and ≈ 80 pct cold reduction. After the first recrystallization treatment, the homogeneity of the alloy composition over the thickness of the slab was verified by electron-probe (X-ray) microanalysis (EPMA). The last cold-rolling step involved about 60 pct thickness reduction. Specimens were cut (geometry: $10 \times 11 \times 0.15$ mm^3) from the rolled strip. They were chemically polished using Kawamura's reagent.[13] The recrystallized specimens were recrystallized at 973 K in H_2 for 45 minutes before nitriding. The grain size of the recrystallized specimen was about 20 μm.

A specimen thickness of 0.1 mm (obtained after treatment with Kawamura's reagent) was used for both the recrystallized and cold-rolled specimens. However, in the case of nitriding at 848 K for the cold-rolled specimens, a thickness of 0.06 mm had to be used to obtain ideally weak interaction behavior (Figure 1, Section III–A).

Nitriding was performed in a thermobalance (DuPont Thermogravimetrical Analyzer (TGA) 951; sensitivity of about 5 μg) using a NH_3/H_2 gas mixture with a nitriding potential r_N ($=p_{NH_3}/(p_{H_2})^{3/2}$) of 2.45×10^{-4} Pa$^{-1/2}$ and

a linear gas velocity of 15.0 mm s^{-1} at temperatures in the range 803 to 853 K for total times varying between 24 and 135 hours (see Reference 14 for a detailed description of gas purification and nitriding in the TGA apparatus). Under these conditions no iron nitrides can be formed. The curves of mass increase shown in the figures were obtained by least-squares spline fitting (polynomial degree of 3) to the data with about 10 breakpoints.

After nitriding, the specimens were annealed at 723 K in pure H_2 to remove the nitrogen that was not chemically bonded (denitriding).

Microhardness profiles were determined by measuring on a cross section using a LEITZ DURIMET* micro-

*LEITZ DURIMET is a trademark of Leitz Inc., Rockleigh, NJ.

Vickers hardness tester with a load of 25 g. Every value for the hardness given in this article represents the average of 10 measurements.

Electron-probe (X-ray) microanalysis (wavelength dispersive analysis) was employed to determine quantitatively the composition and, in particular, to verify that a homogeneous nitrogen distribution was achieved (for details, see Reference 5).

III. RESULTS

A. *Weak Interaction Behavior*

The hardness as a function of depth below the surface for the thin cold-rolled foils is shown in Figure 1. The results obtained show that ideally weak interaction behavior of the solutes Al and N is indeed obtained for the cold-rolled specimens of thickness 0.1 mm. Only at 848 K, a (maximal) thickness of 0.06 mm had to be used in order to guarantee ideally weak interaction behavior. For the case of the recrystallized specimens, it was already shown in Reference 5 that ideally weak interaction behavior holds for specimens with a thickness of 0.3 mm. Therefore, this will certainly be the case for the presently employed thickness of 0.1 mm.

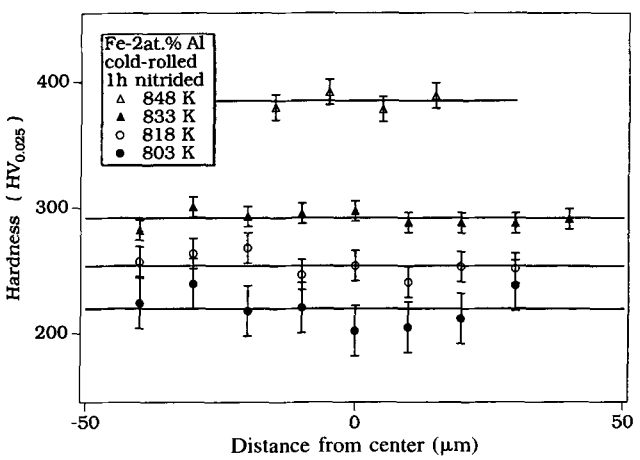

Fig. 1—Hardness-depth profiles of cold-rolled (60 pct thickness reduction) Fe-2 at. pct Al foils after 1 h of nitriding at temperatures indicated. The foil thickness is 100 μm, except for the specimen nitrided at 848 K, which has a thickness of 60 μm (Section III–A). Weak interaction behavior is observed: absence of hardness (composition) gradients.

B. *Thermogravimetric Analysis*

The mass change during gas nitriding in the TGA apparatus is measured as a function of time, t, and temperature, T. The results obtained (after application of correction procedures; Appendix A) are shown in Figures 2 and 3 for the recrystallized and cold-rolled foils, respectively.

The TGA curve of the recrystallized specimen can be subdivided into two stages (Figure 2): (1) saturation of the α-Fe matrix with nitrogen (the nitrogen level at the first plateau corresponds very well with that for saturation of α-Fe[5]) and (2) the nitride-precipitation part of the TGA curves. The TGA curves of the recrystallized specimens show that complete saturation of the matrix with dissolved nitrogen is realized before distinct nitride precipitation becomes apparent (see the first observed plateau in Figure 2). The mass increase characterized by precipitation of AlN shows a sigmoidal-shaped curve

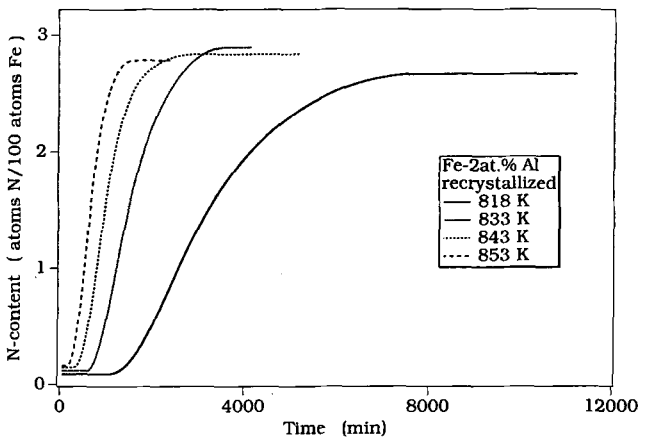

Fig. 2—Nitrogen uptake, expressed as atoms N per 100 atoms Fe, as a function of nitriding time for Fe-2 at. pct Al recrystallized foils nitrided at temperatures indicated. Note the appearance of the first plateau associated with α-Fe matrix saturation with nitrogen.

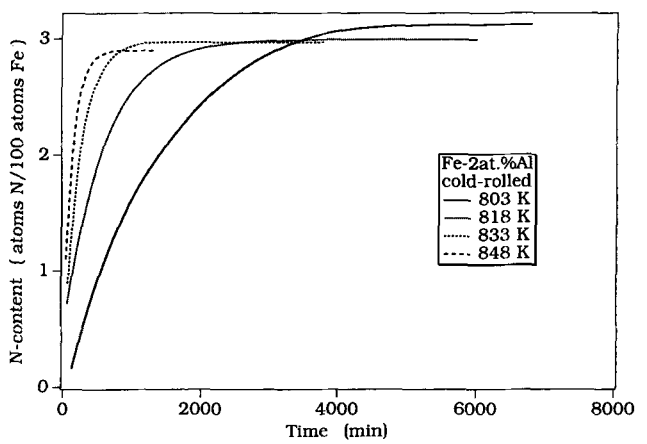

Fig. 3—Nitrogen uptake, expressed as atoms N per 100 atoms Fe, as a function of nitriding time for cold-rolled (60 pct thickness reduction) Fe-2 at. pct Al foils nitrided at temperatures indicated.

Table I. Mass Increase Data for Nitriding of Recrystallized and Cold-Rolled Fe-2 At. Pct Al Specimens*

Nitriding Temperature (K)	Microstructure	$\Delta m_{\text{first plateau}}$ (Atoms N/100 Atoms Fe)	$\Delta m_{\max}$ (Atoms N/100 Atoms Fe)
818	REC	0.09	2.67
833	REC	0.12	2.89
843	REC	0.15	2.84
853	REC	0.16	2.78
803	CR	—	3.12
818	CR	—	3.00
833	CR	—	2.98
848	CR	—	2.90

*$\Delta m_{\text{first plateau}}$ = mass increase corresponding to the first plateau in the curve of mass increase *vs* nitriding time (Figure 2); $\Delta m_{\max}$ = mass increase for completed nitriding (Figure 2).
REC: recrystallized.
CR: cold-rolled.

typical of a solid-state precipitation process controlled by nucleation and growth.[15]

The TGA results obtained for the cold-rolled specimens show that the mass-increase rate is maximal at the start of nitriding and that it decreases continuously to zero (Figure 3). The TGA curves of the cold-rolled specimens do not exhibit a time-separated nitrogen saturation of the matrix (compare Figure 3 with Figure 2).

The mass-increase data for completed nitriding of both recrystallized and cold-rolled materials and for the first plateau observed for the recrystallized specimens are gathered in Table I.

C. *Determination of the Fraction-Transformed AlN*

To separate the effects of matrix saturation and precipitation of aluminum nitride, the degree of precipitation (the fraction transformed), f (with $0 \leq f \leq 1$), can be defined as

$$f = \frac{\Delta m_t - \Delta m_{\alpha\text{-Fe}}}{\Delta m_{\max} - \Delta m_{\alpha\text{-Fe}}} \qquad [1]$$

where Δm_t is the mass increase at time t, $\Delta m_{\alpha\text{-Fe}}$ is the mass increase due to the equilibrium solid solubility of nitrogen in α-Fe, and $\Delta m_{\max}$ is the maximal mass increase.

The curves of fraction transformed *vs* time thus obtained are shown in Figures 4 and 5. In the case of the cold-rolled material, it was assumed that the same mass increase due to matrix saturation with nitrogen can be applied as for the recrystallized material. This implies for cold-rolled material that the matrix saturation with nitrogen has been taken to be realized effectively at t = 0. In view of the relatively large amounts of nitrogen involved in nitride formation, this simplification only introduces a small error for the beginning of transformation. Denitriding after a short time nitriding (20 minutes) at 833 K revealed that not all nitrogen could be removed. Evidently, for the cold-worked condition, nitride precipitation takes place from the start of nitriding.

Apart from the presence of nitrogen incorporated in aluminum nitrides and of nitrogen dissolved in the matrix lattice according to the equilibrium solubility of

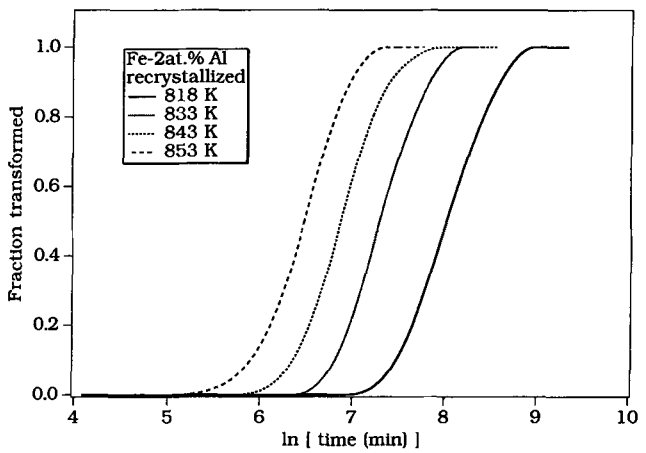

Fig. 4—Fraction AlN precipitated, f, for recrystallized Fe-2 at. pct Al foils as a function of nitriding time at temperatures indicated. Curves obtained from Fig. 2 by application of Eq. [2].

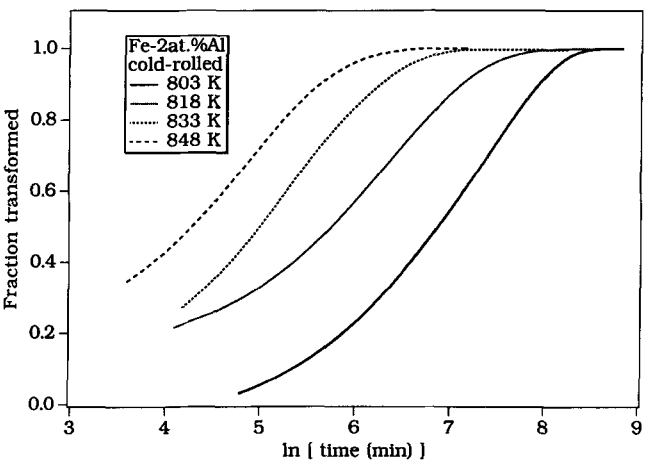

Fig. 5—Fraction AlN precipitated, f, for cold-rolled Fe-2 at. pct Al foils as a function of nitriding time at temperatures indicated. Curves obtained from Fig. 3 by application of Eq. [2].

α-Fe, so-called *excess nitrogen* can occur. The excess nitrogen consists of absorbed nitrogen due to (1) matrix-lattice dilatation caused by (partial) elastic accommodation of the misfit between nitride and matrix, (2) nitrogen adsorbed at the nitride/matrix interfaces, and (3) nitrogen associated with dislocations; for a full discussion, see References 5 and 16, where it has also been shown and explained that the amount of excess nitrogen is only significant for the cold-rolled alloy. In the following discussion (Sections IV, V, and VI) of nitride-precipitation kinetics, the effect of excess nitrogen is considered to be negligible (for the recrystallized alloys) or to be proportional to the momentary amount of nitrogen incorporated in the aluminum nitrides (for the cold-rolled alloys).

IV. METHODS OF KINETIC ANALYSIS

A. *Johnson-Mehl-Avrami Analysis*

For heterogeneous solid-state transformations, often so-called Johnson-Mehl-Avrami (JMA) kinetics are assumed for, in particular, the first stages of precipitation:[15]

$$f(t) = 1 - \exp(-Kt^n) \qquad [2a]$$

with

$$K = K_0 \exp(-Q/RT) \qquad [2b]$$

where K_0 is a pre-exponential factor; Q represents an effective activation energy; n is the JMA exponent; and R and T indicate the gas constant and absolute temperature, respectively.

B. *Activation Energy Determination (AED) Analysis*

The degree of transformation f (with $0 \leq f \leq 1$) can be considered to be determined by a single-state variable β that depends on the path followed in the temperature-time diagram.[17] If the transformation mechanism is invariable for the region in the temperature-time diagram considered, it is tempting to interpret β as proportional to the number of atomic jumps, since T determines the atomic mobility and t defines the duration of the process considered. For an isothermal transformation, it is thus suggested that the state variable β is the product of a rate constant k and transformation time t, where the rate constant obeys an Arrhenius-type relationship:[17]

$$\beta = k(T)t \qquad [3a]$$

with

$$k(T) = k_0 \exp(-E/RT) \qquad [3b]$$

where k_0 is a pre-exponential factor and E denotes an effective activation energy. Without recourse to any kinetic model, a value for the activation energy can be obtained from the lengths of time between two fixed stages of transformation f_1 and f_2, measured at a number of temperatures. It follows that

$$\ln(t_{f_2} - t_{f_1}) = \frac{E}{RT} - \ln k_0 + \ln(\beta_{f_2} - \beta_{f_1}) \qquad [4]$$

A value of E is derived from the slope of a plot of $\ln(t_{f_2} - t_{f_1})$ *vs* $1/T$; a value of k_0 can be obtained from the intercept, provided a specific kinetic model is adopted (implying knowledge of $\beta_{f_2} - \beta_{f_1}$).

It should be noted that the determination of an activation energy for the process studied by application of the AED analysis (Eq. [4]) is more generally valid than by application of JMA analysis (Eq. [2]), because in the AED analysis no specific description is assumed for the dependence of the degree of transformation on time and temperature, in contrast with the JMA analysis.

From a comparison of Eqs. [2] and [3], the following relation between the activation energies defined for the JMA analysis, Q, and the AED analysis, E, is obtained (see also Appendix B in Reference 17):

$$Q = n \times E \qquad [5]$$

Obviously, the experimental values of Q and E are only related through Eq. [5] if the JMA equation provides a satisfactory description for the kinetics of the process considered.

V. NITRIDE PRECIPITATION IN THE RECRYSTALLIZED SPECIMENS

For the recrystallized specimens, the JMA equation (Eqs. [2a] and [2b]) has been fitted simultaneously to the four curves of f *vs* t (one curve per nitriding temperature; Simplex procedure;[18] Figure 4) for $f \leq 0.4$. Results thus obtained for the kinetic parameters K_0, Q, and n are gathered in Table II.

Application of AED (Eq. [4]) to the TGA data of the recrystallized specimens (Figure 4) for $0 \leq f \leq 0.4$ yields the results listed in Table III.

For the present case ($n = 3.7 \pm 0.2$; $Q = 859 \pm 20$ kJ mole^{-1}; Table II), it follows that $Q/n = 232 \pm 14$ kJ mole^{-1}, which well agrees with the experimental value of AED analysis: $E = 248 \pm 10$ kJ mole^{-1} (Table III). This implies that the transformation can be described reasonably well by the JMA formalism (Section IV–B).

The maximal nitride-precipitation rate for the recrystallized material occurs for a progressed stage of nitriding (Figure 4). This is compatible with a heterogeneous transformation process[15] involving precipitation of nitrides governed by nucleation and growth. Along the lines of Reference 19 (Appendix B of Reference 17), if both nucleation and growth occur, the activation energy Q can then be written as

$$Q = (N_{Av} E^* + N_{Av} E_A) + \frac{3}{2} N_{Av} E_D \qquad [6]$$

where E^* is the amount of work associated with nucleation of a (AlN) nucleus of critical size, E_A is the activation energy required for a solute atom (Al) to cross the critical nucleus/matrix interface, and E_D is the activation energy for a diffusional jump to the nearest substitutional vacancy of one solute (Al) atom in the α-Fe matrix. The energies E^* and E_A control the rate of nucleation;[20,21] E_D controls the rate of growth. The factor 3/2 in Eq. [6] expresses that three-dimensional growth

Table II. Values of the Kinetic Parameters Obtained by JMA Analysis (Eq. [2]) Applied to the Recrystallized and Cold-Rolled Fe-2 At. Pct Al Specimens*

Fe-2 At. Pct Al	f range	K_0 (min^{-n})	Q (kJ $mole^{-1}$)	n
Recrystallized	0 to 0.4	$(8 \pm 1) \times 10^{41}$	859 ± 20	3.7 ± 0.2
Cold-rolled	0.4 to 0.9	$(3.0 \pm 0.5) \times 10^{16}$	282 ± 10	1.00 ± 0.03

*K_0 = pre-exponential factor; Q = activation energy; n = JMA exponent.

Table III. Value of the Activation Energy, E, Determined by AED (Eq. [4]) Applied to the Recrystallized and Cold-Rolled Fe-2 At. Pct Al Specimens

Fe-2 At. Pct Al	f range	E (kJ $mole^{-1}$)
Recrystallized	0 to 0.4	248 ± 10
Cold-rolled	0.4 to 0.9	301 ± 10

is assumed with the radial growth of the precipitate proportional to the square root of the diffusion coefficient of aluminum in the matrix. The presence of Avogadro's number, N_{Av}, in Eq. [6] is a consequence of Q (in Eq. [2b]) being expressed as energy per mole.

Taking $N_{Av}E_A = N_{Av}E_D = 196 \pm 10$ kJ $mole^{-1}$[22] and using $Q = 859 \pm 20$ kJ $mole^{-1}$ (Table II), it follows from Eq. [6] that $E^* = (61 \pm 4) \times 10^{-20}$ J. This means that in the case of the recrystallized specimens, the Gibbs free energy barrier for the formation of a critical nucleus of AlN (*i.e.*, $\Delta G^* = (61 \pm 4) \times 10^{-20}\ J \triangleq 369 \pm 26$ kJ $mole^{-1}$, where the effect of a possible entropy term $T\Delta S^*$ is neglected) is not negligible as compared with the chemical Gibbs free energy for formation of AlN with hexagonal crystal structure ($\Delta G_{chem} = -287$ kJ $mole^{-1}$; Table BI).

If the total change in Gibbs free energy on precipitation of AlN is governed by chemical effects and elastic strain effects due to the precipitate/matrix volume misfit, the radius of the critical nucleus, r_0^*, and the associated Gibbs free energy for formation of a critical nucleus, ΔG^*, can be given for a spherical particle as follows (see, for example, Reference 15):

$$r_0^* = -\frac{2\gamma}{\Delta G_{chem} + \Delta G_{strain}} = \sqrt{\frac{3}{4} \times \frac{\Delta G^*}{\pi\gamma}} \qquad [7]$$

$$\Delta G^* = \frac{16\pi}{3} \times \frac{\gamma^3}{(\Delta G_{chem} + \Delta G_{strain})^2} \qquad [8]$$

where γ is the interfacial energy of the interface (per unit area interface), ΔG_{chem} denotes the Gibbs free energy of formation of AlN (per unit volume precipitate) and ΔG_{strain} represents the elastic misfit strain energy in the precipitate/matrix assembly (per unit volume precipitate). Taking the experimental value for ΔG^* ($=61 \times 10^{-20}$ J), ($\Delta G_{chem} + \Delta G_{strain}$) can be plotted *vs* γ (Figure 6).

For further interpretation of Gibbs free energy changes, the composition and the crystal structure of the nitride that precipitates have to be known. Aluminum

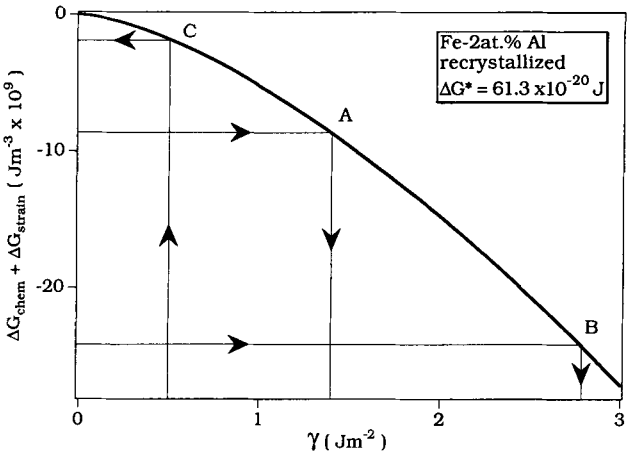

Fig. 6—The sum of the chemical Gibbs free energy, ΔG_{chem}, and the misfit-strain energy, ΔG_{strain}, *vs* the interfacial energy of the interface, γ, for precipitation of a spherical AlN precipitate with $\Delta G^* = 61 \times 10^{-20}$ J as the Gibbs free energy for formation of a nucleus of critical size. Points A and B pertain to precipitation of incoherent, hexagonal AlN with ΔG_{strain} = maximal (point A) and $\Delta G_{strain} = 0$ (point B). Point C pertains to precipitation of coherent, cubic AlN (see text).

nitride is considered as the stoichiometric compound AlN. Two crystal structures for AlN have been indicated (Appendix B in Reference 5). The equilibrium crystal structure of AlN, *i.e.*, the structure to be observed on formation of AlN from the pure elements at normal pressure and temperature (N_2 gas and Al solid), is hexagonal.[23] Hexagonal AlN has a very large volume misfit with the α-Fe matrix. An alternative crystal structure for AlN is the face-centred cubic (fcc) structure,[24] which has a smaller volume misfit with the α-Fe matrix but is expected to have a less negative Gibbs free energy of formation. If AlN precipitates in the hexagonal mode, it will have an incoherent interface with the α-Fe matrix, whereas precipitation of AlN in the fcc mode will be associated with a coherent interface with the α-Fe matrix, at least in the beginning of precipitation.[5] Therefore, in the following, Gibbs free energy calculations for hexagonal AlN are performed assuming an incoherent precipitate/matrix interface, whereas such calculations for cubic AlN are performed assuming a coherent precipitate/matrix interface.

First, the precipitation of incoherent, hexagonal AlN is considered. The formula used for calculation of values of ΔG_{chem} is derived in Appendix B (Table BI). Two extremes for ΔG_{strain} can be indicated for precipitation of hexagonal, incoherent AlN in α-Fe. The volume misfit between precipitate and matrix could be considered as accommodated fully elastically; the corresponding value for ΔG_{strain} is given in Table BIII. However, in view of

the very large value of the misfit, full elastic accommodation is very unlikely, and this value of ΔG_{strain} should be considered as an overestimate. Instead, appreciable misfit-dislocation generation is expected. Accordingly, the volume misfit is largely accommodated plastically; an underestimate for ΔG_{strain}, thus, is nil. Hence, from ΔG_{chem} and ΔG^* and for the range of ΔG_{strain} indicated and using Figure 6 (points A and B), it follows that the surface energy of the interface is in the range 1.4 to 2.7 Jm^{-2}. Indeed, such a surface-energy value corresponds with an incoherent nature of the interface.[25]

Second, the possible precipitation of coherent, cubic AlN is considered. The corresponding value of ΔG_{chem} is unknown. The above treatment can be used to arrive at an estimate for ΔG_{chem} for cubic AlN as follows. If precipitation of cubic AlN in the recrystallized material would occur, an upper estimate for the coherent interfacial energy is 0.5 Jm^{-2}.[26] The misfit-strain energy for this coherent precipitation is given in Table BIII. Taking these energy values, the experimental value for ΔG^* and using Figure 6 (point C), the following underestimate for ΔG_{chem} for cubic AlN is obtained: -69 kJ $mole^{-1}$. Indeed, $|\Delta G_{chem}|$ for cubic AlN is much lower than $|\Delta G_{chem}|$ for hexagonal AlN (see discussion earlier in this section). This value of ΔG_{chem} for cubic AlN will be utilized in Section VI.

The discussion for the situations indicated by points A, B, and C in Figure 6 involves *total* changes of the Gibbs free energy for precipitation in recrystallized α-Fe of either incoherent, hexagonal AlN or coherent, cubic AlN, as presented in Figure 7 as a function of particle size ($\Delta G = \Delta G_{chem} + \Delta G_{strain} + \Delta G_{surf}$, where ΔG_{surf} denotes the contribution due to the precipitate/matrix interfacial energy). Obviously, in the case of the recrystallized specimens, precipitation of incoherent, hexagonal AlN is likely to be favored over precipitation of coherent, cubic AlN.

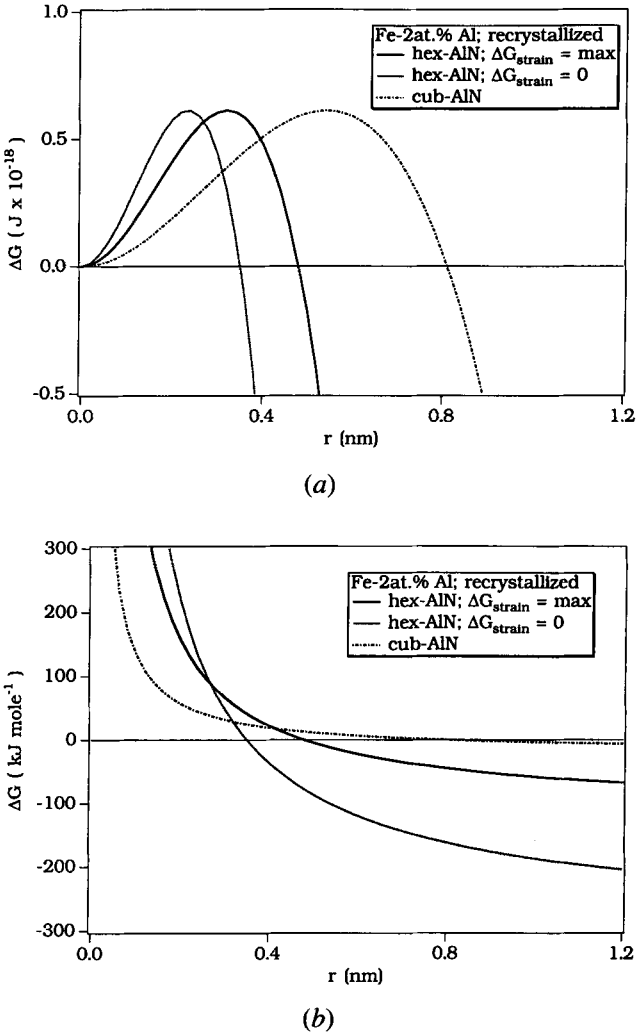

Fig. 7—The total Gibbs free energy change, ΔG, *vs* the radius of a spherical incoherent, hexagonal, or coherent, cubic AlN precipitate, r, calculated for the case of precipitation in recrystallized Fe-2 at. pct Al specimens at 833 K: (*a*) ΔG per particle and (*b*) ΔG per mole of the particle.

VI. NITRIDE PRECIPITATION IN THE DEFORMED SPECIMENS

For the cold-rolled specimens, the JMA equation (Eqs. (2a) and (2b)) has been fitted simultaneously to the four curves of f *vs* t (one curve per nitriding temperature; Simplex procedure;[18] Figure 5) for $0.4 \le f \le 0.9$. Results thus obtained for the kinetic parameters K_0, Q, and n are gathered in Table II.

Application of AED (Eq. [4]) to the TGA data of the cold-rolled specimens (Figure 5) for $0.4 \le f \le 0.9$ yields the results listed in Table III. A good consistency of both values of activation energies occurs: $Q/n = 282 \pm 14$ kJ $mole^{-1}$ and $E = 301 \pm 10$ kJ $mole^{-1}$ (see discussion in Section IV–B).

The value obtained for the JMA exponent ($n = 1.0$) implies formal similarity with "homogeneous reaction kinetics."[15,17] The nitrogen-uptake rate has its maximum value at $t = 0$ and decreases monotonously for $t > 0$. This can be understood as follows. In the cold-rolled material, nucleation sites at dislocations occur abundantly. Thus, most nuclei for nitride precipitation may already be present at, effectively, the start of nitriding. As compared to the recrystallized material, the high density of nuclei in the cold-rolled material implies that the average distance to be covered by solute aluminum atoms before they are incorporated in a nitride particle is much smaller, leading to a much higher nitride-precipitation rate for short nitriding times.

If most nuclei can be assumed to be present effectively at the start of nitriding (see discussion in Sections A and B), it follows (*cf.* Eq. [6]) that

$$Q = \frac{3}{2} N_{Av} E_D \qquad [9]$$

assuming three-dimensional growth as the transformation rate-determining process. According to the experimental data, $Q = 282 \pm 14$ kJ $mole^{-1}$, and thus, $N_{Av} E_D = 188 \pm 10$ kJ $mole^{-1}$. This value agrees well with the activation energy for volume diffusion of aluminum in an α-Fe matrix (196 ± 10 kJ $mole^{-1}$[22]).

The above interpretation of Q implies that AlN formation in the cold-rolled Fe-2 at. pct Al alloy proceeds

as a growth process for the major part of the precipitation. The observation of an apparently weak interaction behavior of the solutes Al and N for the case of cold-rolled alloys (Section I) for sufficiently thin foils may then be understood as follows.

In cold-worked metallic specimens, the dislocation density can be in the range 10^{15} to 10^{16} m/m^3, which corresponds with an average separation of dislocation lines of 10 to 30 nm. For the Fe-2 at. pct Al alloy, it holds that the average distance between the aluminum atoms is about 1 nm. Therefore, at the start of nitriding, (at least) one per 10 to 30 aluminum atoms resides on a dislocation line (ignoring a possible segregation). Apparently, upon inward diffusion of nitrogen, those aluminum atoms on dislocations can lead to instantaneous formation of nitride nuclei (because there is no energy barrier for nucleus formation). Continued nitriding implies both (1) diffusion of nitrogen to larger depths and (2) diffusion of aluminum toward the already existing nitride nuclei. As a result, for a sufficiently thin (for nitrogen to reach the core of the specimen) foil, a homogeneous nitrogen concentration increasing with the stage of nitriding can be observed (*cf.* Figure 1). Note that strong interaction behavior of the alloying element and nitrogen implies occurrence of a nitriding rate decreasing with nitriding time, as observed here, but in contrast with the results obtained here, in that case, diffusion of nitrogen governs the precipitation process, and all aluminum at a certain depth should be converted at once in nitride.[5,11]

The precipitation of new phase particles on dislocations can lead to (partial) release of the elastic strain energy associated with the line defects, which promotes the heterogeneous character of the precipitation process. If a specific volume misfit occurs between precipitate and matrix, the unfavorable effect of the associated strain energy for the precipitate/matrix assembly has to be considered as well (as in Section V). Then, in the case of precipitation on dislocations, an additional, normally favorable (depending on the relative positions of dislocation and precipitate) effect of the release of elastic strain energy by the interaction of the precipitate/matrix-misfit and dislocation stress fields has to be taken into account.

In general the Gibbs free energy change for precipitation on/along a dislocation line, ΔG, can be given as:

$$\Delta G = \Delta G_{chem} + \Delta G_{surf} + \Delta G_{strain} - \Delta G_{disl} + \Delta G_{int} \quad [10]$$

where ΔG_{chem} = Gibbs free energy of formation for the precipitate;
ΔG_{surf} = precipitate/matrix interfacial energy;
ΔG_{strain} = elastic strain energy of matrix and precipitate;
ΔG_{disl} = released part of dislocation-line energy; and
ΔG_{int} = interaction energy of precipitate/matrix and dislocation stress fields.

Two extremes can be considered:[27] incoherent[20,28] and coherent[29,30] precipitates of various shapes. In the following, the Gibbs free energy change for precipitation of AlN on dislocations will be calculated semi-quantitatively for incoherent, hexagonal AlN and coherent, cubic AlN.

A. *Incoherent Precipitation*

The formation of a cylindrical, elastically isotropic precipitate of radius r around the dislocation line in an elastically isotropic matrix is considered. Unlike as in the original article,[28] here the occurrence of a distinct misfit-strain energy is accounted for; the interaction energy is ignored (which is fully justified for precipitation on screw dislocations[31]). The formation of the incoherent precipitate releases all the elastic energy initially stored in the volume it occupies, *i.e.*, the dislocation energy within the precipitate volume is completely relaxed. The energy change ΔG per unit length of dislocation line then becomes (*cf.* Eq. [10])

$$\Delta G = \pi r^2(\Delta G_{chem} + \Delta G_{strain}) + 2\pi r\gamma_{incoh} - A \ln(r/r_{core}) \quad [11]$$

where ΔG_{chem} and ΔG_{strain} (for the *incoherent* precipitate) hold per unit volume of precipitate; γ_{incoh} is the interfacial energy per unit surface; and A equals $Gb^2/[4\pi(1-\nu)]$ for edge dislocations and $Gb^2/4\pi$ for screw dislocations, with G and ν as shear modulus and Poission's constant of the matrix, respectively, and b as the length of the Burgers vector (r_{core} is the radius of the dislocation core, say $r_{core} \approx 0.1$ nm[32]).

The value of the radius of the critical nucleus, r^*_{disl}, is calculated from $d(\Delta G)/dr = 0$. The result is (*cf.* References 15 and 28)

$$r^*_{disl} = \frac{1}{2} r^*_0 + \frac{1}{2}\sqrt{(r^*_0)^2 + \frac{2A}{\pi(\Delta G_{chem} + \Delta G_{strain})}} \quad [12a]$$

with

$$r^*_0 = -\frac{\gamma_{incoh}}{(\Delta G_{chem} + \Delta G_{strain})} \quad [12b]$$

The factor r^*_0 represents the radius of the critical nucleus for homogeneous precipitation in the matrix. Since $A > 0$ and $(\Delta G_{chem} + \Delta G_{strain}) < 0$, $r^*_{disl} < r^*_0$. From Eqs. [12a] and [12b], it follows that if

$$(\Delta G_{chem} + \Delta G_{strain}) < -\pi\gamma^2_{incoh}/2A \quad [12c]$$

then r^*_{disl} has no finite real value, and an activation-energy barrier for precipitation on the dislocation, ΔG^*_{disl}, does not occur for $r^*_{disl} > r_{core}$. For the case of precipitation of incoherent, hexagonal AlN, ΔG_{chem} is given in Table BI. The maximal value of ΔG_{strain} for a cylindrical incoherent precipitate of hexagonal AlN is given in Table BIII, which holds if the volume misfit is accommodated fully elastically (which is very unlikely; see Section V). If the volume misfit is accommodated partially plastically, ΔG_{strain} is smaller. As in Section V, the minimal estimate for ΔG_{strain} is taken as nil. As estimates for the interfacial energies, the values obtained in Section V are adopted: 2.7 Jm^{-2} for the maximal value of ΔG_{strain} and 1.4 Jm^{-2} for $\Delta G_{strain} = 0$. Now taking $A = Gb^2/[4\pi(1-\nu)]$ with $G = 81.6 \times 10^9$ Jm^{-3}, $b = 0.25 \times 10^{-9}$ m, and $\nu = 0.28$,[33] it then follows that the criterion [12c] is always satisfied, *i.e.*, an activation-energy barrier for nucleation does not occur.

B. *Coherent Precipitation*

The formation of a coherent precipitate in general does not lead to a release of all the elastic energy, as dislocation-line energy, initially stored in the volume it occupies (if the elastic constants of both matrix and precipitate are equal and both matrix and precipitate are elastically isotropic, even nothing of this energy will be liberated: $\Delta G_{disl} = 0$). However, the interaction energy of the precipitate/matrix and dislocation stress fields can favor precipitation around or along dislocations. ΔG_{int} can be made negative by proper positioning of the precipitate: this implies that the precipitate should develop in the compressive part or the tensile part of the strain field surrounding an edge dislocation, depending on the volume misfit between precipitate and matrix being negative or positive. For the case of precipitation of a cylindrical, elastically isotropic precipitate of radius r along an edge dislocation in the elastically isotropic matrix, with equal elastic constants for matrix and precipitate, it then follows for the energy change ΔG per unit length of dislocation (*cf.* Eq. [10]):

$$\Delta G = \pi r^2(\Delta G_{chem} + \Delta G_{strain}) + 2\pi r\gamma_{coh} - B\pi r \quad [13]$$

where ΔG_{chem} and ΔG_{strain} (for the *coherent* precipitate) hold per unit volume of precipitate and γ_{coh} is the interfacial energy per unit surface. The term $B\pi r$ denotes the combined effects of $-\Delta G_{disl}$ and ΔG_{int} (for the case considered, $\Delta G_{disl} = 0$). If the cylindrical precipitate is tangent to the dislocation line, the cylinder axis is in the plane defined by the half-plane of the edge dislocation considered, and the precipitate is either on the compressive side for $\varepsilon < 0$ or on the tensile side for $\varepsilon > 0$ (where ε is the linear misfit parameter, as described in Appendix B), then B is given by (*cf.* References 27 and 29):

$$B = \frac{Gb}{\pi} \cdot \frac{(1+\nu)}{(1-\nu)} \cdot |\varepsilon| \quad [14]$$

The value of the radius of the critical nucleus, r^*_{disl}, corresponding to a maximum in the curve of ΔG *vs* r, thus satisfies

$$r^*_{disl} = r^*_0 + \frac{B}{2(\Delta G_{chem} + \Delta G_{strain})} \quad [15a]$$

with

$$r^*_0 = -\frac{\gamma_{coh}}{(\Delta G_{chem} + \Delta G_{strain})} \quad [15b]$$

where r^*_0 represents the radius of the critical nucleus for homogeneous precipitation. Precipitation of hexagonal AlN in a coherent fashion is very unlikely. For coherent cubic AlN it follows that since $B > 0$ and $(\Delta G_{chem} + \Delta G_{strain}) < 0$ (an assessment of ΔG_{chem} is given earlier in this section; for ΔG_{strain}, see Table BIII), $r^*_{disl} < r^*_0$. From Eqs. [15a] and [15b], it can further be concluded that if

$$B > 2\gamma_{coh} \quad [15c]$$

then an r^*_{disl} does not exist and an activation-energy barrier for precipitation does not occur.

Taking B as in Eq. [14] with G, b, and ν as in Section A, it is calculated from the previous criterion that γ_{coh} should be smaller than 0.7 Jm^{-2}. This condition is easily met in practice for coherent interfaces.[26] Thus, it is conceivable that coherent nucleation of fcc AlN on dislocations takes place without an activation-energy barrier.

For the energy models for precipitation of both incoherent, hexagonal AlN and coherent, cubic AlN, according to Eqs. [11] and [13], respectively, the Gibbs free energy change can be calculated as a function of precipitate radius r. The results are shown in Figure 8. Although the calculations for incoherent, hexagonal AlN indicate that no activation-energy barrier exists for a nucleation of precipitate with a radius larger than the radius of the core of the dislocation, it should be concluded that, from the observation that $\Delta G > 0$ for small r ($>r_{core}$) and the realization that $\Delta G = 0$ for $r = 0$, the nucleation of incoherent, hexagonal AlN in fact has to be associated with an activation-energy barrier (see dashed lines in Figure 8(a) for $r < r_{core}$), albeit experienced at a very small particle size.

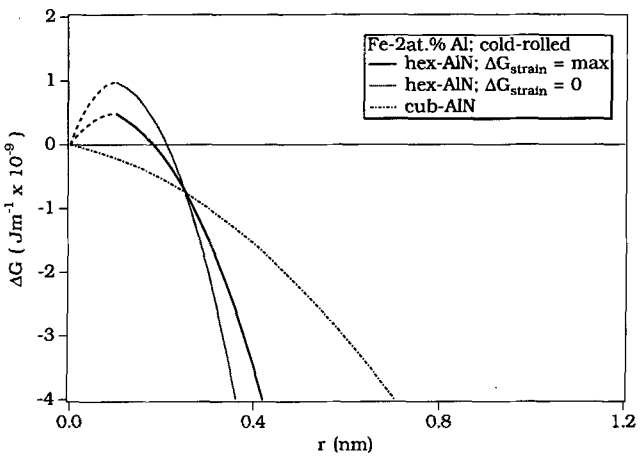

(*a*)

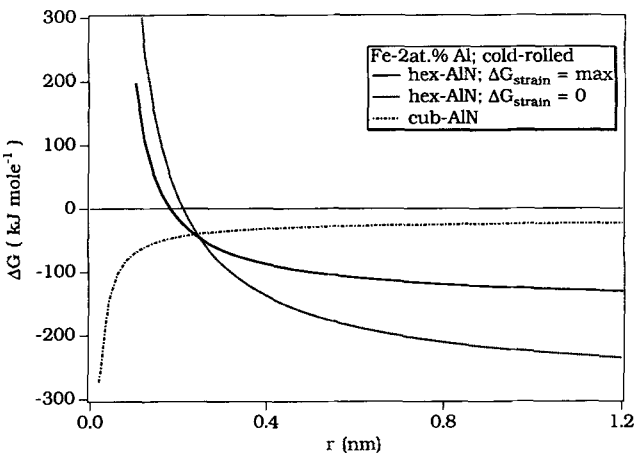

(*b*)

Fig. 8—The total Gibbs free energy change, ΔG, *vs* the radius of a cylindrical incoherent, hexagonal, or coherent, cubic AlN precipitate, r, calculated for the case of precipitation on/along a dislocation line in cold-rolled Fe-2 at. pct Al specimens at 833 K: (*a*) ΔG per particle and per unit length of dislocation and (*b*) ΔG per mole of the particle.

Clearly, in the beginning of precipitation, the precipitation of coherent, cubic AlN ($\Delta G < 0$ for all precipitate radii) is favored over precipitation of incoherent, hexagonal AlN ($\Delta G > 0$ for small precipitate radii). This is consistent with the actual observation of fcc AlN precipitates in nitrided cold-rolled Fe-Al alloys.[34] The calculations suggest that at more advanced stages of precipitation/particle growth, the incoherent, hexagonal mode becomes energetically more stable than the coherent, cubic mode (Figure 8). A precise prediction of this stage, in terms of the particle size at which the incoherent, hexagonal form becomes preferred, cannot be made on the basis of the current assessment: the models and calculations are approximate (in particular, the estimation of ΔG_{chem} for cubic AlN, performed in Section V, is likely to be subject to large uncertainty). Further, if the transition from the cubic to the hexagonal mode actually takes place for the precipitate size predicted, it is also determined by kinetic factors: the rearrangement of Al and N atoms required may be associated with one or more (additional) activation-energy barriers.

The specific Gibbs free energy changes on precipitation in the recrystallized and cold-rolled specimens cannot be compared directly from Figures 7(a) and 8(a), where the energy change *per particle formed* is shown as a function of particle size. Therefore, the Gibbs free energy changes are shown *per mole precipitate formed* in Figures 7(b) and 8(b). It is clear that only for small precipitate size, as in the beginning of precipitation, the effect of the presence of dislocations is pronounced; for advanced stages of particle growth, the chemical and misfit-strain contributions obviously govern the Gibbs free energy change for formation of AlN.

VII. CONCLUSIONS

The kinetics of precipitation of aluminum nitride in recrystallized and cold-rolled Fe-2 at. pct Al alloy differ vastly.

A. *Recrystallized Specimens*

1. The precipitation of AlN is rate controlled by both nucleation and growth (the maximal nitride-precipitation rate occurs for a progressed stage of nitriding).
2. In terms of Johnson-Mehl-Avrami kinetics, the activation energy for the nitriding process is 859 ± 20 kJ mole^{-1}.
3. A significant Gibbs free energy barrier is observed for the formation of a nucleus of AlN of critical size: (61 ± 4) × 10^{-20} J per nucleus = 369 ± 26 kJ mole^{-1}; *i.e.*, it is of the same order of magnitude as the negative of the chemical Gibbs free energy of nitride formation.
4. Considering chemical, interfacial, and precipitate strain-field contributions to the total change in Gibbs free energy on precipitation, it follows that precipitation of incoherent, hexagonal AlN is favored over precipitation of coherent, cubic AlN.

B. *Cold-Rolled Specimens*

1. The precipitation of AlN is rate controlled by growth (the maximal nitride-precipitation rate occurs at the beginning of nitriding).
2. In terms of Johnson-Mehl-Avrami kinetics, the total activation energy for the nitriding process is 282 ± 10 kJ mole^{-1}. It follows that volume diffusion of aluminum in the α-Fe matrix provides the nitriding rate-determining step.
3. A Gibbs free energy barrier for the formation of a nucleus of AlN of critical size does not occur.
4. Considering chemical, interfacial, and precipitate and dislocation strain-field contributions to the total change in Gibbs free energy on precipitation on/along a dislocation, it follows that the precipitation of coherent, cubic AlN is favored over precipitation of incoherent, hexagonal AlN, at least in the beginning of the precipitation process. It is conceivable that for advanced stages of particle growth, the incoherent, hexagonal variant of AlN precipitate is more stable energetically.

APPENDIX A

Correction applied to mass-increase (TGA) curve

In the thermobalance used in the present experiments (DuPont TGA 951), the ferromagnetic specimen is heated by an alternating current (AC) coil. The coil is not compensated, and a net electromagnetic field results. On heating up of a ferromagnetic specimen to the annealing temperature of an isothermally conducted experiment the induction effect generated by the electromagnetic field leads to a force exerted on the specimen. As a consequence, the balancing specimen can take a slightly different position with respect to the mass detection device, and a different mass value is read. The mass may shift to an apparently negative value, supposing mass = 0 corresponds to the mass reading before heating up. Therefore, the mass increase recorded at the end of the treatment, Δm_{tot}^{TGA}, is set equal to the value obtained according to a separate weighing experiment employing a mechanical Mettler balance (with an accuracy of 1 μg), Δm_{tot}^{Mett}. Hence,

$$\Delta m_{tot}^{Mett} = \Delta m_{tot}^{TGA} \quad [A1]$$

and

$$m_{t=0}^{TGA} = m_{tot}^{TGA} - \Delta m_{tot}^{Mett} \quad [A2]$$

where m_{tot}^{TGA} is the mass reading of the TGA apparatus at the end of the treatment and $m_{t=0}^{TGA}$ is the deduced mass reading according to the TGA experiment at the beginning of the isothermal annealing. Then, the mass increase at time t, $(\Delta m_t)'$, according to the scale of TGA apparatus, reads

$$(\Delta m_t)' = m_t^{TGA} - m_{t=0}^{TGA} = m_t^{TGA} - m_{tot}^{TGA} + \Delta m_{tot}^{Mett} \quad [A3]$$

where m_t^{TGA} denotes the mass reading at time t of the TGA apparatus.

Although the procedure corresponding to Eq. [A3] was employed, it was found that the mass increase corresponding with the first plateau in the TGA curves of

the recrystallized specimens (Figure 2 and Section III), $(\Delta m_t)'_{\text{first plateau}}$, did not comply with the solid solubility of nitrogen in α-Fe, in contrast with what was expected (Appendix A of Reference 5). This effect is ascribed to (electronic) drift. This led to a (second) correction applied to the TGA data of the recrystallized specimens.

To verify that the first plateau in the TGA curve recorded for the recrystallized specimens indicates the nitrogen uptake to realize the nitrogen solubility of the ferrite matrix, a few additional experiments were carried out. A specimen was heated up to the nitriding temperature in an H_2 gas flow. After a constant reading for the mass was established,* the desired nitriding potential was imposed by replacing the H_2 flow by a NH_3/H_2 flow of the selected composition. After about 3 hours of nitriding, the experiment was stopped (the first plateau in the TGA curves was reached after about 1 hour in all experiments and 3 hours of nitriding was always smaller than the time after which distinct precipitation occurred; the mass increase was determined by applying a Mettler microbalance (with an accuracy of 1 μg). This experiment was performed at two different nitriding temperatures (818 and 833 K). The results on the nitrogen solubility in α-Fe, $[N]_{\alpha\text{-Fe}}$, thus obtained experimentally and calculated from the data in Reference 3 are gathered in Table AI. The experimentally determined data for $[N]_{\alpha\text{-Fe}}$ agree well with the predicted ones, within experimental accuracy.

*Stabilizing of the nitriding temperature (indicated by a constant value read for the mass) took about 25 minutes.

Then, for all experiments performed with the recrystallized specimens, the mass readings by the TGA apparatus have to be adapted such that the first plateau corresponds with the mass increase for realization of nitrogen saturation of matrix, $\Delta m_{\alpha\text{-Fe}}$. The first step of this correction is a shift of the $(\Delta m_t)'$ scale to a $(\Delta m_t)'_1$ scale with $(\Delta m_t)'_1 = (\Delta m_t)' - (\Delta m_t)'_{\text{first plateau}}$. Hence, $(\Delta m_t)'_1 = 0$ indicates the nitrogen uptake corresponding with the first plateau in mass increase due to nitrogen solubility in α-Fe. Then, the unit of the mass scale is changed by multiplication with A1 according to

$$\text{A1} = \left\{ \frac{\Delta m_{\text{tot}}^{\text{Mett}} - \Delta m_{\alpha\text{-Fe}}}{\Delta m_{\text{tot}}^{\text{Mett}} - (\Delta m_t)'_{\text{first plateau}}} \right\} \qquad [A4]$$

This leads to a mass scale $(\Delta m_t)'_2$ given by $(\Delta m_t)'_2 = \text{A1} \cdot (\Delta m_t)'_1$. Now, the $(\Delta m_t)'_2$ data < 0 are ignored, and a shift of the $(\Delta m_t)'_2$ scale to the Δm_t scale with $\Delta m_t = (\Delta m_t)'_2 + \Delta m_{\alpha\text{-Fe}}$ is realized. This implies that Δm_{tot} is equal to $\Delta m_{\text{tot}}^{\text{Mett}}$. Summarizing,

$$\Delta m_t = [-\text{A1} \cdot (\Delta m_t)'_{\text{first plateau}} + \Delta m_{\alpha\text{-Fe}}] + \text{A1} \cdot (\Delta m_t)' \qquad [A5]$$

APPENDIX B

Chemical and misfit-strain Gibbs free energy contributions on precipitation of AlN

1. *Chemical Gibbs Free Energy for the Formation of AlN in α-Fe*

The precipitation of AlN from aluminum and nitrogen dissolved in ferrite (α-Fe), denoted by Al_α and N_α, respectively, can be written as

$$Al_\alpha + N_\alpha \leftrightarrows AlN_\alpha \qquad [B1]$$

The chemical Gibbs free energy change on precipitation of one mole AlN, indicated with ΔG_{chem}, can be given as

$$\Delta G_{\text{chem}} = G^0_{(\text{AlN})_\alpha} - G^0_{\text{Al}_\alpha} - G^0_{\text{N}_\alpha} + RT \ln a_{(\text{AlN})_\alpha} - RT \ln a_{\text{Al}_\alpha} - RT \ln a_{\text{N}_\alpha} \qquad [B2]$$

where the superscript 0 refers to the standard state for the compound/element concerned and the activities, a, are defined with respect to the corresponding standard states.

If the pure compound/pure elements are adopted as standard states, and thus, $G^0_{(\text{AlN})_\alpha} = G^0_{\text{AlN}}$, $a_{(\text{AlN})_\alpha} = 1$, $G^0_{\text{Al}_\alpha} = G^0_{\text{Al}}$ (Al = solid Al), and $G^0_{\text{N}_\alpha} = (1/2)G^0_{\text{N}_2}$ (N_2 = N_2 gas), it follows that

$$\Delta G^f_{\text{AlN}} \equiv G^0_{\text{AlN}} - G^0_{\text{Al}} - \frac{1}{2} G^0_{\text{N}_2} = G^0_{(\text{AlN})_\alpha} - G^0_{\text{Al}_\alpha} - G^0_{\text{N}_\alpha} \qquad [B3]$$

with ΔG^f_{AlN} as the so-called Gibbs free energy of formation of AlN (from the pure elements). Note that the G^0 terms and, thus, ΔG^f_{AlN} depend on temperature.

If the solution of Al in α-Fe is diluted, implying that the atomic fraction $x_{\text{Al}_\alpha} \ll 1$, the regular solution model may be applied and the activity a_{Al_α} approximately obeys:[26]

$$RT \ln a_{\text{Al}_\alpha} = RT \ln x_{\text{Al}_\alpha} + \Omega_{\text{Al/Fe}} \qquad [B4]$$

with $\Omega_{\text{Al/Fe}}$ as the interaction parameter that is related to the heat of mixing (Al dissolving in α-Fe), $\Delta H_{\text{Al}\to\text{Fe}}$, according to

$$\Delta H_{\text{Al}\to\text{Fe}} = x_{\text{Al}_\alpha} \cdot (1 - x_{\text{Al}_\alpha}) \cdot \Omega_{\text{Al/Fe}} \approx x_{\text{Al}_\alpha} \cdot \Omega_{\text{Al/Fe}} \qquad [B5]$$

If nitriding is performed in a NH_3/H_2 gas mixture, the activity a_{N_α} is related to the equilibrium

$$NH_3 \leftrightarrows N_\alpha + \frac{3}{2} H_2 \qquad [B6]$$

according to

$$RT \ln a_{\text{N}_\alpha} = G^0_{\text{NH}_3} - \frac{3}{2} G^0_{\text{H}_2} - G^0_{\text{N}_\alpha} + RT \ln \frac{p_{\text{NH}_3}}{p^{3/2}_{\text{H}_2}} \qquad [B7]$$

Table AI. Mass Data for Recrystallized Fe-2 At. Pct Al Specimens of Initial Mass m_0*

T (K)	m_0 (mg)	$\Delta m^{\text{exp}}_{\alpha\text{-Fe}}$ (mg)	$[N]^{\text{exp}}_{\alpha\text{-Fe}}$ (Atoms N/100 Atoms Fe)	$\Delta m^{\text{th}}_{\alpha\text{-Fe}}$ (mg)	$[N]^{\text{th}}_{\alpha\text{-Fe}}$ (Atoms N/100 Atoms Fe)
818	88.055	0.027	0.12	0.024	0.11
833	104.597	0.034	0.13	0.033	0.13

*$\Delta m^{\text{exp}}_{\alpha\text{-Fe}}$ and $[N]^{\text{exp}}_{\alpha\text{-Fe}}$ indicate the experimentally determined (Mettler balance) nitrogen solubility of the matrix as obtained from the first plateau (Figure 2); $\Delta m^{\text{th}}_{\alpha\text{-Fe}}$ and $[N]^{\text{th}}_{\alpha\text{-Fe}}$ indicate the corresponding predicted value using data from Reference 3.

Table BI. The Chemical Gibbs Free Energy for Formation of Hexagonal AlN in α-Fe, $\Delta G_{chem}^{AlN\text{-}hex}$*

Temperature (K)	ΔG^f_{AlN} (kJ mole^{-1})	$RT \ln a_{Al_\alpha}$ (kJ mole^{-1})	$RT \ln a_{N_\alpha}$ (kJ mole^{-1})	$\Delta G_{chem}^{AlN\text{-}hex}$ (kJ mole^{-1})	$\Delta G_{chem}^{AlN\text{-}hex}$ (J m^{-3} × 10^{10})
803	−232	35	22	−289	−2.30
818	−230	34	23	−287	−2.29
833	−229	34	25	−288	−2.29
843	−227	34	26	−287	−2.28
848	−227	34	26	−287	−2.28
853	−226	33	27	−286	−2.28
858	−226	33	27	−286	−2.28

*ΔG^f_{AlN} is the Gibbs free energy for formation of AlN from the pure elements; a_{Al_α} and a_{N_α} are the activities of Al and N dissolved in α-Fe before AlN precipitation, respectively; R is the gas constant; and T is the absolute temperature.

Table BII. Data Used for Calculation of the Misfit-Strain Energy for Formation of AlN in α-Fe, ΔG_{strain}

	α-Fe	AlN-hex	AlN-cubic
Lattice parameter (nm)	$a = 0.28664$[41]	$a = 0.3111$[23] $c = 0.4978$[23]	$a = 0.407$[24]
Molar volume, V (m^3 mole^{-1})	7.091 × 10^{-6}	12.563 × 10^{-6}	10.150 × 10^{-6}
Misfit parameter, ε*		0.21	0.13
Poisson's constant, ν	0.28[33]		
Shear modulus, G (GPa)	81.6[33]		
Bulk modulus, K (GPa)	158	198**	202**
C*		0.65	0.65

*Using relations in Appendix B, Section 2–A.
**Using elastic constants from Reference 39 and Eq. [B10].

Table BIII. The Misfit-Strain Energy for Formation of AlN in α-Fe, ΔG_{strain}

Incoherent, Hexagonal AlN (Eq. [B9])				Coherent, Cubic AlN (Eq. [B11])	
Sphere		Cylinder			
(kJ mole^{-1})	(J m^{-3} × 10^{10})	(kJ mole^{-1})	(J m^{-3} × 10^{10})	(kJ mole^{-1})	(J m^{-3} × 10^{10})
176	1.40	132	1.05	50	0.49

The standard state for N_α has been taken such that $G^0_{N_\alpha} = 1/2\ G^0_{N_2}$. Thus, it follows (see Reference 35) that

$$\Delta G^f_{NH_3} = G^0_{NH_3} - \frac{3}{2} G^0_{H_2} - \frac{1}{2} G^0_{N_2}$$

$$= G^0_{NH_3} - \frac{3}{2} G^0_{H_2} - G^0_{N_\alpha} \qquad [B8]$$

Note that $\Delta G^f_{NH_3}$, the Gibbs free energy change for formation of NH_3 from N_2 and H_2, is temperature dependent.

Values for ΔG^f_{AlN} and $\Delta G^f_{NH_3}$ are taken from literature sources.[35,36] A value for $\Omega_{Al/Fe}$ is obtained by adopting the one pertaining to dissolving liquid Al in liquid Fe as derived from the corresponding heat of dissolution (data from Reference 37). Obviously, x_{Al}, p_{NH_3}, and p_{N_2} are taken as applied in the nitriding experiment (Section II). A summary of numerical data and contributions to ΔG_{chem} (Eq. [B2]) is given in Table BI.

The resulting values for ΔG_{chem} for precipitation of hexagonal AlN are gathered in Table BI (only for hexagonal AlN literature values for ΔG^f_{AlN} exist; for cubic AlN, a value of ΔG_{chem} is estimated in Section V); for the temperature range considered, there is only a very minor temperature dependence of ΔG_{chem}.

2. *Misfit-Strain Energy for the Formation of AlN in α-Fe*

A. *Incoherent precipitation*

The misfit-strain energy in the precipitate (B)/matrix (A) assembly for an incoherent precipitate can be given per mole precipitate by[15]

$$\Delta G^{incoh}_{strain} = 6 \cdot G_A \cdot C \cdot \varepsilon^2 \cdot V_B \cdot E(y/R) \qquad [B9]$$

with

$$\varepsilon = \left(\frac{(V^0_B)^{1/3} - (V^0_A)^{1/3}}{(V^0_A)^{1/3}} \right);$$

$$C = \frac{3K_B}{(3K_B + 4G_A)}; \qquad V_B = (1 + C\varepsilon)^3 \cdot V^0_A$$

where G_A is the shear modulus of the matrix; V^0_A and V^0_B are the molar volumes of the matrix and precipitate in the unstrained state, respectively; K_B is the bulk modulus of the precipitate, and $E(y/R)$ is a shape factor (for the particle taken as an ellipsoid with y and R as its semiaxes). For incompressible precipitates, $E(y/R) = 1$ for a sphere and $E(y/R) = 3/4$ for a cylinder.[38]

Hexagonal AlN can be considered as an elastically isotropic material. This follows from the single-crystal elastic constants of hexagonal AlN[39] applied to the elastical isotropy condition (refer to Table 9 at p. 140 from Reference 40). For elastically isotropic material (and always for material of cubic crystal symmetry), the bulk modulus of elasticity is given by[40]

$$K = \frac{1}{3}(c_{11} + 2c_{12}) \qquad [B10]$$

where c_{11} and c_{12} are elastic stiffnesses. The bulk modulus of hexagonal AlN thus calculated is given in Table BII.

The misfit-strain energy for formation of hexagonal, incoherent AlN in α-Fe was calculated for spherical and cylindrical precipitates using Eq. [B9] and the data in Table BII, thereby adopting as estimates for the shape factor $E(y/R)$ the data from Reference 38; the results are shown in Table BIII.

B. *Coherent precipitation*

The misfit-strain energy in the precipitate/matrix assembly for a coherent precipitate can be given per mole precipitate by[15]

$$\Delta G_{\text{strain}}^{\text{coh}} = 2 \cdot G \cdot \frac{1+\nu}{1-\nu} \cdot \varepsilon^2 \cdot V_B \qquad [B11]$$

with ν as the Poisson constant and where the elastic constants of precipitate and matrix have been taken equal (note that for the initial, coherent stage of a precipitation process, the elastic constants for the minute precipitates can differ largely from their bulk values). This result is independent of the shape of the precipitate.

The misfit-strain energy for formation of cubic, coherent AlN in α-Fe was calculated using Eq. [B11] and the data in Table BII; the result is shown in Table BIII.

ACKNOWLEDGMENTS

We are obliged to Mr. J.S. Steenaert and Dr. Ir. M.A.J. Somers for stimulating discussions. We are indebted to Messrs. P.F. Colijn and Ing. N. Geerlofs for skillful experimental and technical support. These investigations in the program of the Foundation for Fundamental Research on Matter (FOM) have been supported (in part) by the Netherlands Technology Foundation (STW).

REFERENCES

1. E.J. Mittemeijer: in *Case-Hardened Steels: Microstructural and Residual Stress Effects*, D.E. Diesburg, ed., TMS-AIME, Warrendale, PA, 1984, p. 161; *Härterei-Technol. Mitt.*, 1984, vol. 39, p. 16.
2. K. Bohnenkamp: *Arch. Eisenhüttenwes.*, 1967, vol. 38, p. 433.
3. H.H. Podgurski and H.E. Knechtel: *Trans. AIME*, 1969, vol. 245, p. 1595.
4. H.H. Podgurski, R.A. Oriani, and F.N. Davis: *Trans. AIME*, 1969, vol. 245, p. 1603.
5. M.H. Biglari, C.M. Brakman, M.A.J. Somers, W.G. Sloof, and E.J. Mittemeijer: *Z. Metallkd.*, 1993, vol. 84, p. 124.
6. E.T. Turkdogan and S. Ignatowicz: *J. Iron Steel Inst.*, 1958, vol. 188, p. 242.
7. B.J. Lightfoot and D.H. Jack: *Proc. Heat Treatment*, The Metals Society, London, 1973, p. 59.
8. J.R. Atanasova: *Härterei-Technol. Mitt.*, 1976, vol. 31, p. 325.
9. R.E.E. Pulkkinen: *Met. Sci.*, 1982, vol. 16, p. 37.
10. R.E.E. Pulkkinen: *Scan. J. Metall.*, 1983, vol. 12, p. 87.
11. P.M. Hekker, H.C.F. Rozendaal, and E.J. Mittemeijer: *J. Mater. Sci.*, 1985, vol. 20, p. 718.
12. P.C. van Wiggen, H.C.F. Rozendaal, and E.J. Mittemeijer: *J. Mater. Sci.*, 1985, vol. 20, p. 4561.
13. K. Kawamura: *J. Jpn. Inst. Met.*, 1960, vol. 24, p. 710.
14. M.A.J. Somers, N.M. van der Pers, D. Schalkoord, and E.J. Mittemeijer: *Metall. Trans. A*, 1989, vol. 20A, pp. 1533-39.
15. J.W. Christian: *The Theory of Transformations in Metals and Alloys*, 2nd ed. Pergamon Press, Oxford, 1975.
16. M.H. Biglari, C.M. Brakman, E.J. Mittemeijer, and S. van der Zwaag: Delft University of Technology, unpublished research, 1994.
17. E.J. Mittemeijer: *J. Mater. Sci.*, 1992, vol. 27, p. 3977.
18. W.H. Press, B.P. Flannery, S.A. Teukolsky, and W.T. Vetterling: *Numerical Recipes*, Cambridge University Press, New York, NY, 1987, p. 289.
19. R.M. Lankreijer, M.A.J. Somers, and E.J. Mittemeijer: *Proc. Int. Conf. on High Nitrogen Steels*, Lille, May 18–20, 1988, J. Foct and A. Hendry, eds., The Institute of Metals, London, 1989, p. 108.
20. R. Gomez-Ramirez: Ph.D. Thesis, Stanford University, Stanford, CA, 1971.
21. R. Gomez-Ramirez and G.M. Pound: *Metall. Trans. A*, 1973, vol. 4A, pp. 1563-70.
22. M. Gemmaz, M. Afyouni, and A. Mosser: *Surf. Sci. Lett.*, 1990, vol. 227, p. L109.
23. G.A. Jeffrey and V.Y. Wu: *Acta Crystallogr.*, 1963, vol. 16, p. 559.
24. S. Hanai, N. Takemoto, and Y. Mizuyama: *Trans. Iron Steel Inst. Jpn.*, 1971, vol. 11, p. 24.
25. T. Utigard: *Z. Metallkd.*, 1993, vol. 84, p. 792.
26. D.A. Porter and K.E. Easterling: *Phase Transformation in Metals and Alloys*, Van Nostrand Reinhold, London, 1989.
27. F.C. Larché: in *Dislocations in Solids*, F.R.N. Nabarro, ed., North-Holland Publishing Co., Amsterdam, 1979, p. 135.
28. J.W. Cahn: *Acta Metall.*, 1957, vol. 5, p. 169.
29. B.Ya. Lyubov and V.A. Solov'Yev: *Fiz. Metal. Metalloved.*, 1965, vol. 19, p. 333.
30. C.C. Dollins: *Acta Metall.*, 1970, vol. 18, p. 1209.
31. L. Katgerman and J. Van Liere: *Acta Metall.*, 1978, vol. 26, p. 361.
32. J.P. Hirth and J. Lothe: *Theory of Dislocations*, MacGraw-Hill, New York, NY, 1968, p. 63.
33. C.J. Smithells: *Metals Reference Book*, 5th ed., Butterworths, London, 1976.
34. M.H. Biglari, C.M. Brakman, E.J. Mittemeijer, and S. van der Zwaag: Delft University of Technology, unpublished research, 1994.
35. E.J. Mittemeijer and J.T. Slycke: *Härterei-Technol. Mitt.*, in press.
36. I. Barin: *Thermochemical Data of Pure Substances*, Cambridge University Press, New York, NY, 1989.
37. R. Hultgren, P.D. Desai, D.T. Hawkins, M. Gleiser, and K.K. Kelley: *Selected Values of the Thermodynamic Properties of Binary Alloys*, ASM Metals Park, OH, 1973, p. 162.
38. F.R.N. Nabarro: *Proc. R. Soc.*, 175, vol. A, 1940, p. 519.
39. M.E. Sherwin and T.J. Drummond: *J. Appl. Phys.*, 1991, vol. 69, p. 8423.
40. J.F. Nye: *Physical Properties of Crystals*, Oxford University Press, Oxford, 1989, p. 140.
41. W.B. Pearson: *A Handbook of Lattice Spacings and Structure of Metals*, Pergamon Press, London, 1968, vol. II.